

Article

Biosensor Based on Covalent Organic Framework Immobilized Acetylcholinesterase for Ratiometric Detection of Carbaryl

Ying Luo, Na Wu, Linyu Wang, Yonghai Song, Yan Du  and Guangran Ma *

National Engineering Research Center for Carbohydrate Synthesis, Key Lab of Fluorine and Silicon for Energy Materials and Chemistry of Ministry of Education, College of Chemistry and Chemical Engineering, Jiangxi Normal University, Nanchang 330022, China

* Correspondence: grma@jxnu.edu.cn or guangranma2008@163.com; Tel.: +86-0791-88120861

Abstract: A ratiometric electrochemical biosensor based on a covalent organic framework (COF_{Thi-TFPB}) loaded with acetylcholinesterase (AChE) was developed. First, an electroactive COF_{Thi-TFPB} with a two-dimensional sheet structure, positive charge and a pair of inert redox peaks was synthesized via a dehydration condensation reaction between positively charged thionine (Thi) and 1,3,5-triformylphenylbenzene (TFPB). The immobilization of AChE on the positively charged electrode surface was beneficial for maintaining its bioactivity and achieving the best catalytic effect; therefore, the positively charged COF_{Thi-TFPB} was an appropriate support material for AChE. Furthermore, the COF_{Thi-TFPB} provided a stable internal reference signal for the constructed AChE inhibition-based electrochemical biosensor to eliminate various effects which were unrelated to the detection of carbaryl. The sensor had a linear range of 2.2–60 μM with a detection limit of 0.22 μM , and exhibited satisfactory reproducibility, stability and anti-interference ability for the detection of carbaryl. This work offers a possibility for the application of COF-based materials in the detection of low-level pesticide residues.

Keywords: carbaryl; acetylcholinesterase; covalent organic framework; inhibition-based electrochemical biosensor



Citation: Luo, Y.; Wu, N.; Wang, L.;

Song, Y.; Du, Y.; Ma, G. Biosensor

Based on Covalent Organic

Framework Immobilized

Acetylcholinesterase for Ratiometric

Detection of Carbaryl. *Biosensors*

2022, 12, 625. [https://doi.org/](https://doi.org/10.3390/bios12080625)

10.3390/bios12080625

Received: 18 July 2022

Accepted: 8 August 2022

Published: 10 August 2022

Publisher's Note: MDPI stays neutral with regard to jurisdictional claims in published maps and institutional affiliations.



Copyright: © 2022 by the authors. Licensee MDPI, Basel, Switzerland. This article is an open access article distributed under the terms and conditions of the Creative Commons Attribution (CC BY) license (<https://creativecommons.org/licenses/by/4.0/>).

1. Introduction

Carbaryl as a kind of carbamate pesticide has been widely applied in agricultural products due to their short-term toxicity and high insecticidal activity [1–4]. However, because of the bioaccumulation effect, a large amount of residual carbaryl in water, soil, food and the environment enter the human body through the skin, respiratory tract, digestive tract, etc., resulting in irreversible damage [5–8]. Therefore, it is crucial to achieve rapid detection and reliable quantification of carbaryl. Traditional detection methods, such as chromatography [9–12], surface-enhanced Raman spectroscopy [13–15], immunoassay [16,17], etc., have been developed very well, with high sensitivity and accuracy in the determination of pesticide residues in water and agricultural products. However, the limitations lie in the complex sample handling process, the use of highly toxic organic solvents and the expensive and complex instruments that require professional testing [18–20].

Nowadays, acetylcholinesterase (AChE) inhibition-based electrochemical biosensors have attracted great attention with regard to the detection of carbaryl and other carbamate pesticides due to their advantages of non-toxicity, simplicity, miniaturized, high specificity and high sensitivity [21–23]. For example, Loguercio et al. established the biosensor for the detection of carbaryl by immobilizing AChE on the polypyrrole nanocomposite, showing satisfactory results [24]. Zhang et al. used graphene as the support material to load AChE, and the constructed sensor realized the chiral recognition of (+)/(–)-methamidophos [25]. Considering that acetic acid, the hydrolysate of acetylthiocholine (ATCh), can induce the collapse of unstable metal-organic frameworks (MOFs), Li et al. prepared a biodegradable

ZIF-8/MB composite using the one-pot method and realized ultrasensitive detection of paraoxon by using AChE as the recognition molecule [26]. The mechanism of the AChE inhibition-based electrochemical biosensors is that the carbamate pesticides make the serine residue hydroxyl group of the AChE catalytic center be carbamylated, resulting in a decrease in its activity or even making it completely inactive. Thus, the catalytic hydrolysis of ATCh is weakened, leading to a decrease in the production of thiocholine (TCh). The response current of TCh is inversely proportional to the concentration of carbamate pesticides such as carbaryl; therefore, this causes the simple, efficient and sensitive detection of carbaryl [27–31].

The following two points are of great significance for the construction of high-performance AChE inhibition-based pesticide electrochemical sensors. Firstly, choose an appropriate support material to immobilize the enzyme and maintain its activity [32–34]. Suitable electrode support materials should allow a large number of enzymes to be loaded and provide a good microenvironment for maintaining enzyme activity [35–37]. Yang et al. reported that fixing AChE on the support material with a positive charge not only favors the maintenance of its bioactivity, but also promotes electron transport between the AChE and electrode surface [38]. Secondly, the influence of the background current and changeable environmental conditions on sensor performance should be avoided [39–41]. The traditional single-signal electrochemical sensors have low accuracy and sensitivity and poor reproducibility because their electrochemical signal is easily affected by the background current of the workstation and environmental conditions such as temperature and pH [42,43]. Fortunately, dual-signal ratiometric electrochemical sensors have emerged [44–46]. Wang et al. coated an electroactive covalent organic framework ($\text{COF}_{\text{Thi-TFPB}}$) on the surface of carbon nanotubes (CNTs) using the one-pot method, and the prepared $\text{COF}_{\text{Thi-TFPB}}$ -CNT nanocomposite was used for electrochemical ratiometric detection of AA. Since the monomer thionine (Thi) was positively charged, the positively charged $\text{COF}_{\text{Thi-TFPB}}$ could self-peel into large-sized two-dimensional crystal nanosheets, and a pair of redox peaks of the $\text{COF}_{\text{Thi-TFPB}}$ was inert to the detection of AA; thus, it could be used as a reference signal [47].

Here, an electrochemical sensor based on the $\text{COF}_{\text{Thi-TFPB}}$ [48–51] loaded with AChE for the detection of carbaryl is proposed. The positively charged $\text{COF}_{\text{Thi-TFPB}}$ can be easily stripped into two-dimensional nanosheets, and modified on the surface of a bare glassy carbon electrode (GCE) without adhesives or conductive agents. The positively charged $\text{COF}_{\text{Thi-TFPB}}$ is conducive to effectively maintaining the bioactivity of AChE and achieving the best catalytic effect. Its inherent redox peak at 0/−0.22 V is inert to the detection of carbaryl, which could be used as a reference signal to further improve the sensitivity and accuracy of the detection. The prepared sensor shows good reproducibility, stability and anti-interference ability. This work proposes an efficient strategy to immobilize enzymes using an electroactive COF as a support material.

2. Experimental Procedure

2.1. Materials and Reagents

1,3,5-triformylphenylbenzene (TFPB) and thionine (Thi) were purchased from Jilin Yanshen Technology Co., Ltd., (Beijing, China). N,N-dimethylformamide (DMF), N,N-dimethylacetamide (DMA), mesitylene, tetrahydrofuran (THF), acetic acid (AcOH), acetylcholinesterase (AChE), acetylthiocholine (ATCh) and other chemicals were purchased from Inokay Co., Ltd. (Beijing, China). Carbaryl was purchased from Mokai Nike Technology Co., Ltd. (Jiangxi, China).

2.2. Instruments

Scanning/transmission electron microscopy images (SEM/TEM) were obtained via the HITACHI S-3400N SEM and JM-2010 (HR) TEM (Chiyoda City, Japan), respectively. Atomic force microscopy (AFM) images were obtained via the instrument model BRUKER Nanoscope V (MultiMode 8) (Billerica, MA, USA) multifunctional scanning probe micro-

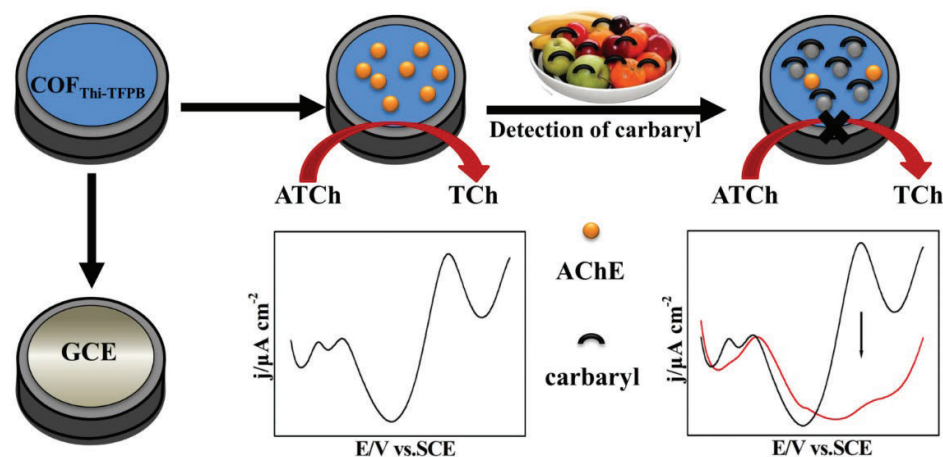
scope. Fourier transform infrared spectroscopy (FTIR) was recorded on model Perkin-Elmer Spectrum 100 spectrometer (Waltham, MA, USA). N_2 adsorption/desorption isotherm measurements were operated using a BELSORP-mini II instrument (Microtrac, Haan/Duesseldorf, Germany) under the liquid nitrogen temperature of 77 K. Powder X-ray diffraction (XRD) analysis was performed on the D/Max 2500 V/PC X-ray powder diffractometer (Rigaku, Tokyo, Japan) with a scanning step of $1^\circ/\text{min}$. All electrochemical studies were performed on an electrochemical workstation (CHI 760D, Shanghai, China).

2.3. Preparation of $COF_{\text{Thi-TFPB}}$

Firstly, 0.2 mM TFPB and 0.3 mM Thi were added to a mixture with 2 mL of 1,4-dioxane, and 1 mL of mesitylene and DMF, and ultrasound was performed for 15 min. Next, it was transferred to a 25 mL reaction kettle with 0.2 mL (concentration: 6 M) acetic acid (used as an initiator), and placed in an oven at 120°C for three days. Finally, the dark-blue $COF_{\text{Thi-TFPB}}$ was obtained by centrifugation and freeze-drying [52].

2.4. Preparation of $AChE/COF_{\text{Thi-TFPB}}/GCE$

Firstly, the surface of the glassy carbon electrode (GCE) was treated with Al_2O_3 , ethanol and ultrapure water until smooth and clean. Then, $5\ \mu\text{L}$ of the $2\ \text{mg/mL}$ $COF_{\text{Thi-TFPB}}$ was dropped on the electrode surface. After drying, $AChE/COF_{\text{Thi-TFPB}}/GCE$ was prepared by dropping 0.4 mM AChE on the modified electrode. The detection mechanism of carbaryl is shown in Scheme 1.



Scheme 1. Schematic illustration for the detection mechanism of carbaryl.

3. Results and Discussion

3.1. Characterization of $COF_{\text{Thi-TFPB}}$

SEM (Figure 1a), TEM (Figure 1b) and AFM (Figure 1c) showed that the $COF_{\text{Thi-TFPB}}$ owned a film-like lamellar structure, and the thickness was about 1.42 nm, which was very favorable for the immobilization of AChE [53,54]. Next, an FTIR spectrum and XRD pattern were used to demonstrate the successful synthesis of the $COF_{\text{Thi-TFPB}}$. The spectrum of the $COF_{\text{Thi-TFPB}}$ showed that a new peak of $-C=N-$ appeared at $1658\ \text{cm}^{-1}$, whereas the disappearance of $N-H$ in $-NH_2$ at $3292\ \text{cm}^{-1}$ and $C=O$ in $-CHO$ at $1689\ \text{cm}^{-1}$. Meanwhile, the stretching vibration peaks corresponding to $-CH$ in $-CHO$ at $2714\ \text{cm}^{-1}$ and $2834\ \text{cm}^{-1}$ disappeared. These results demonstrated that the $COF_{\text{Thi-TFPB}}$ was synthesized successfully (Figure 1d). The XRD pattern further confirmed the successful synthesis of the crystalline $COF_{\text{Thi-TFPB}}$ (Figure 1e). Diffraction peaks at 6.67° , 8.48° , 11.34° , 25.8° and 45.6° corresponded to (100), (110), (210), (152) and (111) crystal planes. The N_2 adsorption/desorption isotherm of the $COF_{\text{Thi-TFPB}}$ showed that the specific surface area was $67.4\ \text{m}^2\ \text{g}^{-1}$ (Figure 1f).

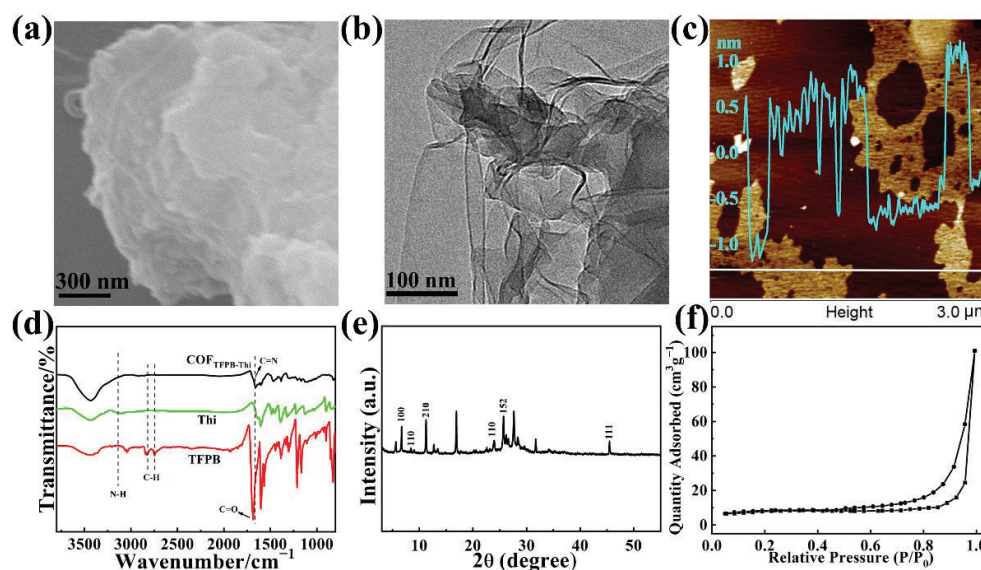


Figure 1. SEM, TEM and AFM images of $\text{COF}_{\text{Thi-TFPB}}$ (a–c). FTIR spectrum (d), XRD pattern (e) and N_2 adsorption/desorption isotherm (f) of $\text{COF}_{\text{Thi-TFPB}}$.

3.2. Electrochemical Behaviors of $\text{COF}_{\text{Thi-TFPB}}/\text{GCE}$ and $\text{AChE}/\text{COF}_{\text{Thi-TFPB}}/\text{GCE}$

To successfully construct an electrochemical sensor for ratiometric detection of carbaryl, the introduced internal reference signal should have good stability and a suitable oxidation potential. Therefore, the electrochemical performance of the $\text{COF}_{\text{Thi-TFPB}}$ was evaluated by cyclic voltammetry (CV). As shown in Figure 2a, compared with the TFPB/GCE (b) without a peak, both the $\text{COF}_{\text{Thi-TFPB}}/\text{GCE}$ (c) and Thi/GCE (a) had two pairs of redox peaks at the same potential, indicating that the peaks on the $\text{COF}_{\text{Thi-TFPB}}/\text{GCE}$ came from the electroactive Thi. Next, the CV of the $\text{COF}_{\text{Thi-TFPB}}/\text{GCE}$ was investigated at different scan rates. It could be seen that the positions of their redox peaks were basically unchanged with the increase in scanning rate (Figure 2b). The redox peak at $-0.2/-0.07$ V was caused by the electrochemical reaction of Thi in the $\text{COF}_{\text{Thi-TFPB}}$, and the redox peak at $0/-0.22$ V was due to the conjugated structure of Thi in the $\text{COF}_{\text{Thi-TFPB}}$ [55]. With the increase in scanning rate, the peak current density of the two redox peaks of the $\text{COF}_{\text{Thi-TFPB}}$ also increased and showed a good linear relationship, indicating that the reaction process was a typical surface control process (Figure 2c). Based on the linear regression equation between the anodic/cathodic peak potential and natural logarithm of the scan rate (Figure 2d), it could be calculated that the electron-transfer number (n) was 1, and the electron-transfer coefficient (α_s) was 0.369 when the redox potential was $0/-0.22$ V [56].

Then, CV and electrochemical impedance spectroscopy (EIS) tests were performed using $5.0 \text{ mM } [\text{Fe}(\text{CN})_6]^{3-/4-}$ in a 0.1 M KCl solution as a probe to investigate the electrochemical behaviors of the $\text{COF}_{\text{Thi-TFPB}}/\text{GCE}$ and $\text{AChE}/\text{COF}_{\text{Thi-TFPB}}/\text{GCE}$. As shown in Figure 3a, compared with the bare GCE (curve a), the peak current of $[\text{Fe}(\text{CN})_6]^{3-/4-}$ on the $\text{COF}_{\text{Thi-TFPB}}/\text{GCE}$ (curve b) was slightly increased, and the peak-to-peak potential difference was slightly decreased. This result might be attributed to the electrostatic attraction between the negative $[\text{Fe}(\text{CN})_6]^{3-/4-}$ and the positive $\text{COF}_{\text{Thi-TFPB}}$. In the meantime, the redox peak of $[\text{Fe}(\text{CN})_6]^{3-/4-}$ on the $\text{AChE}/\text{COF}_{\text{Thi-TFPB}}/\text{GCE}$ (curve c) owned the smallest peak current and the largest peak-to-peak potential difference. It was mainly due to the poor conductivity of AChE, which would hinder the electron transport between $[\text{Fe}(\text{CN})_6]^{3-/4-}$ and the surface of the electrode [57,58]. The charge transfer resistance (R_{ct}) values of the bare GCE, $\text{COF}_{\text{Thi-TFPB}}/\text{GCE}$ and $\text{AChE}/\text{COF}_{\text{Thi-TFPB}}/\text{GCE}$ were 31.3Ω , 8.5Ω and 288.1Ω , respectively (Figure 3b). In conclusion, compared with the $\text{COF}_{\text{Thi-TFPB}}/\text{GCE}$, the peak current of $[\text{Fe}(\text{CN})_6]^{3-/4-}$ on the $\text{AChE}/\text{COF}_{\text{Thi-TFPB}}/\text{GCE}$ decreased and the R_{ct} value increased, which directly proved the successful fixation of AChE on the $\text{COF}_{\text{Thi-TFPB}}/\text{GCE}$.

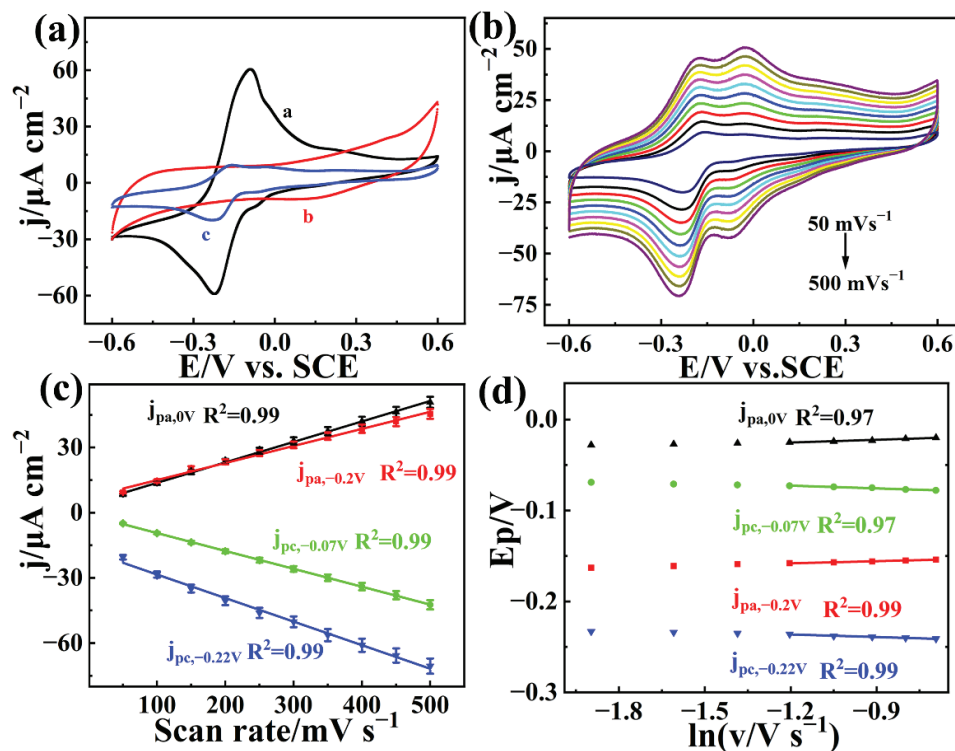


Figure 2. (a) CV of TFPB/GCE (curve b), Thi/GCE (curve a) and COF_{Thi-TFPB}/GCE (curve c) in 0.1 M N₂-saturated PBS (pH = 7.0). (b) CVs of COF_{Thi-TFPB}/GCE at different scan rates (50 mV s⁻¹ to 500 mV s⁻¹) in 0.1 M N₂-saturated PBS (pH = 7.0). (c) The corresponding fitting curves between current density and scan rates. (d) The corresponding fitting curves between E_p and ln v.

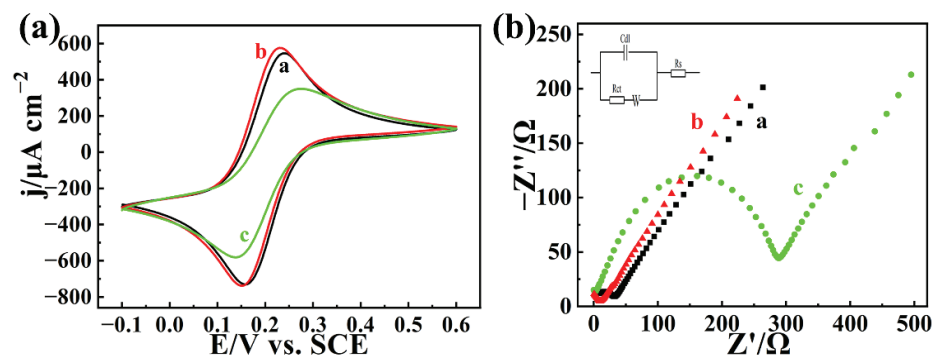


Figure 3. (a) CVs and (b) EIS of bare/GCE (curve a) and COF_{Thi-TFPB}/GCE (curve b), AChE/COF_{Thi-TFPB}/GCE (curve c) in 0.1 M KCl solution with 5.0 mM [Fe(CN)₆]^{3-/4-}. Inset in b is its equivalent circuit.

3.3. Optimization of the Experimental Conditions

It was known that when at the optimum pH value, the binding ability of the enzyme molecule to the substrate was the strongest and the enzyme reaction rate was the highest; however, if the pH was too large or too small, the enzyme might be inactivated [59,60]. Therefore, the pH value of the solution was optimized. As shown in Figure 4a, when pH = 7.0, the current density of the AChE/COF_{Thi-TFPB}/GCE was the largest in the 0.1 M PBS with 0.6 mM ATCh and 5 μM carbaryl. Then, the amount of the COF_{Thi-TFPB} modified on the electrode surface was optimized (Figure 4b), which showed that the optimal volume was 5 μL (concentration: 2 mg/mL). Next, considering that the amount of loaded AChE and the concentration of substrate molecule ATCh had important influence on the detection results, they were also optimized. It could be observed that it was best to set the concentration of AChE and ATCh at 0.4 mM and 0.6 mM in the subsequent experiments,

respectively (Figure 5a,b). Figure 5c showed the relationship between the catalytic activity inhibition of AChE and the incubation time. The inset is the formula for calculating the percentage of inhibition ($I\%$), where $j_{P,control}$ was the original current density recorded by the AChE/COF_{Thi-TFPB}/GCE in 0.1 M PBS (pH = 7.0) with 0.6 mM ATCh, $j_{P,exp}$ was the residual current density recorded after immersing in 0.1 M PBS (pH = 7.0) with 0.6 mM ATCh and 5 μ M carbaryl for 0, 4, 8, 12, 16, 20 and 30 min. All in all, when the concentration of AChE was 0.4 mM, ATCh was 0.6 mM and the incubation time was 20 min, the performance of the AChE/COF_{Thi-TFPB}/GCE sensor was the best.

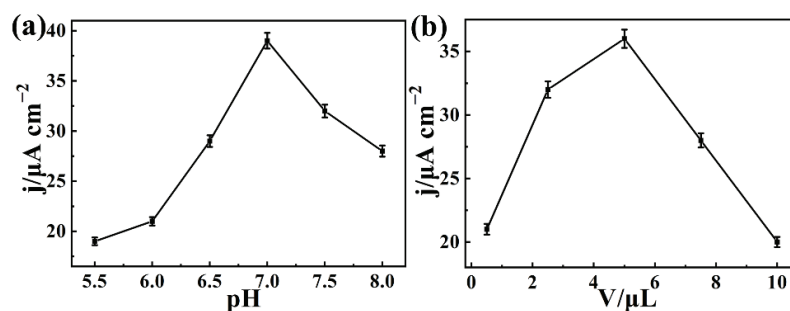


Figure 4. The plots of peak current density versus different pH (a) and different volumes of COF_{Thi-TFPB} (b).

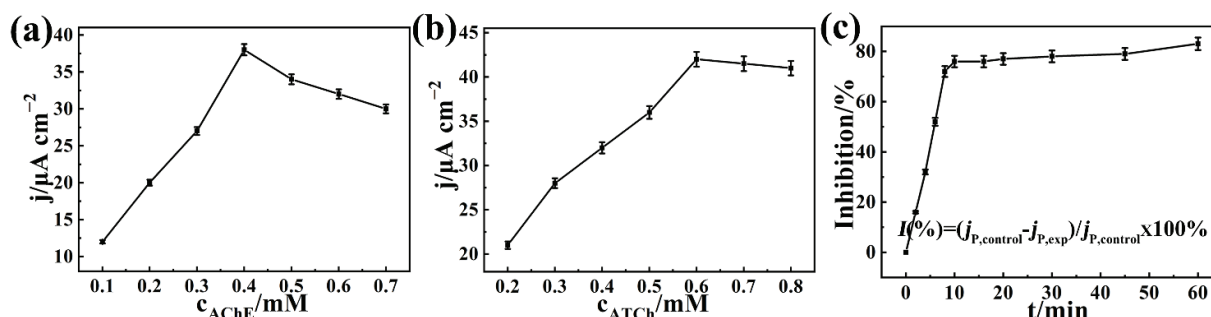


Figure 5. The plots of peak current density versus different concentrations of AChE (a), different concentrations of ATCh (b) and different incubation times (c).

3.4. Electrochemical Detection of Carbaryl Based on AChE/COF_{Thi-TFPB}/GCE

Firstly, the affinity of AChE fixed on the COF_{Thi-TFPB} to ATCh was investigated. Figure 6a shows the relation curve between response current density and time after continuously adding ATCh. It could be seen that there was a good linear relationship between the oxidation peak current density and the concentration of ATCh between 0.01 mM and 0.27 mM. However, the slow-response current density at higher concentrations of ATCh indicated a Michaelis–Menten process. According to the slope and intercept of the linear regression equation in Figure 6b, the Michaelis–Menten constant (K_m) was calculated to be 0.24 mM. This value was lower than 0.622 mM as measured by the AChE/COF@MWCNTs/GCE [61], suggesting good affinity between the enzyme and the substrate. Then, a ratiometric electrochemical sensor based on the AChE/COF_{Thi-TFPB} was used to detect carbaryl in 0.1 M PBS (pH = 7.0) containing 0.6 mM ATCh. As shown in Figure 7a, the peak current density of the COF_{Thi-TFPB} at -0.05 V was basically unchanged with the addition of carbaryl, whereas the peak current density of TCh at 0.6 V gradually decreased. This was because the toxic effect of carbaryl on AChE led to a decrease in the amount of TCh, and then, the electrochemical signal was weakened. The inset in Figure 7a shows the linear relationship between j_{TCh}/j_{COF} and the concentration of carbaryl, where the linear range of the carbaryl sensor was 2.2–60 μ M and the detection limit was 0.22 μ M. The performance of the AChE/COF_{Thi-TFPB}/GCE sensor was compared with other sensors (Table 1). It could be seen that the detection limit of this sensor was lower than that based on Au/PAMAM/GLUT/AChE (3.2 μ M) and MWCNT/PANI/AChE (1.4 μ M).

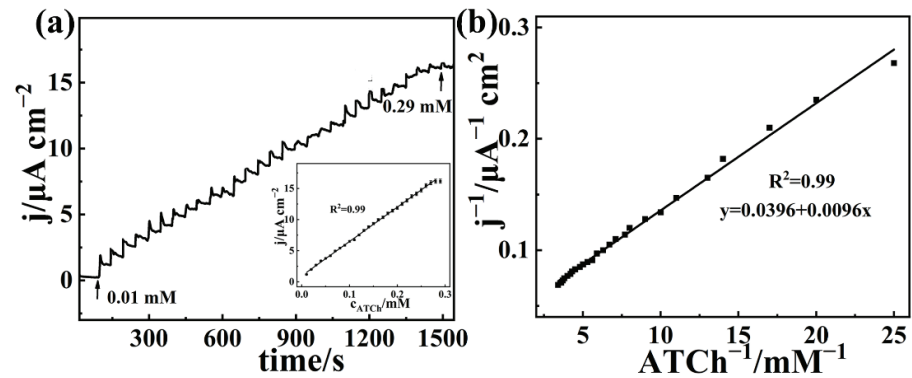


Figure 6. (a) Amperometric response current density for AChE/COF_{Thi-TFPB}/GCE obtained by continuously adding ATCh in 0.1 M PBS (pH = 7.0) with constant stirring at a voltage set to 0.7 V. Inset: the plots of response current density versus different concentrations of ATCh. (b) The Lineweaver-Burk plot.

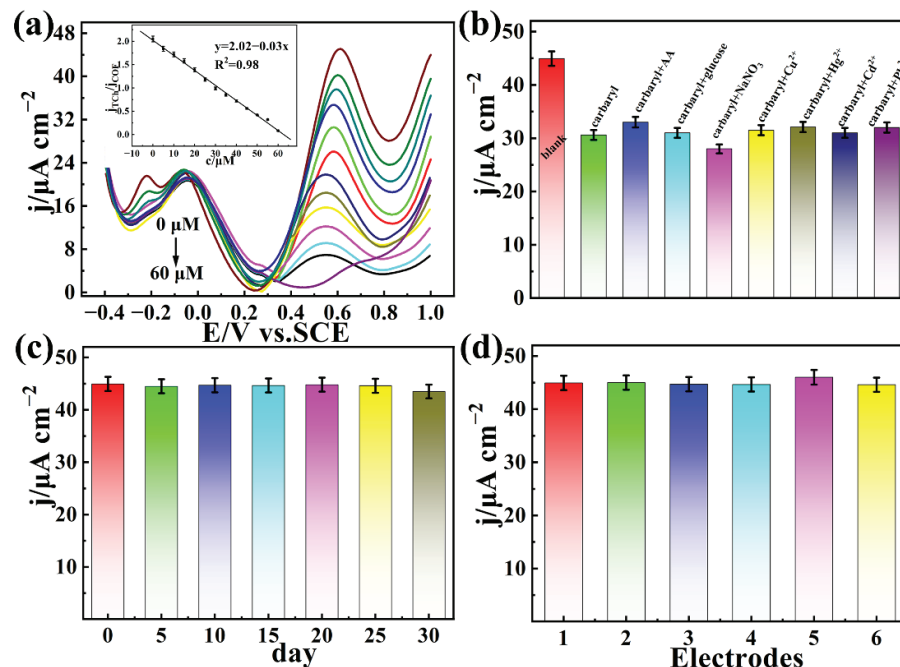


Figure 7. (a) The DPV response of AChE/COF_{Thi-TFPB}/GCE in 0.1 M PBS (pH = 7.0) containing 0.6 mM ATCh with different concentrations of carbaryl. (Inset: fitting curve between current density and the concentration of carbaryl). (b) The selectivity of AChE/COF_{Thi-TFPB}/GCE in 0.1 M PBS (pH = 7.0) with 0.6 mM ATCh, 10 μM carbaryl and 50 μM interferences. (c,d) The stability and reproducibility of AChE/COF_{Thi-TFPB}/GCE in 0.1 M PBS (pH = 7.0) with 0.6 mM ATCh and 5 μM carbaryl.

The selectivity of the AChE/COF_{Thi-TFPB}/GCE sensor was investigated in 0.1 M PBS (pH = 7.0) with 0.6 mM ATCh, 10 μM carbaryl and 50 μM interferences. It could be seen that these interferences had little effect on the peak current density (Figure 7b). Then, one AChE/COF_{Thi-TFPB}/GCE was used to measure the corresponding peak current density of 5 μM carbaryl in 0.1 M PBS (pH = 7.0) with 0.6 mM ATCh for 30 days. The relative standard deviation (RSD) was only 1.15%, indicating that the AChE/COF_{Thi-TFPB}/GCE sensor had good stability (Figure 7c). The RSD of 5 μM carbaryl detected by six independent AChE/COF_{Thi-TFPB}/GCEs was 1.45% in 0.1 M PBS (pH = 7.0) with 0.6 mM ATCh (Figure 7d). The good stability and reproducibility might be attributed to the fact that the positively charged COF_{Thi-TFPB} could immobilize the AChE enzyme and maintain its activity, and its oxidation peak played a self-correcting role in the detection of carbaryl.

Table 1. Performance comparison of several carbaryl electrochemical sensors.

Electrode	LOD (μM)	Linear Range (μM)	Reference
GC/rGO/AChE	0.0019	0.2–10	[62]
Au/PAMAM/GLUT/AChE	3.2	1–9	[63]
Nafion/AChE/CHIT/IAM	0.004	0.005–5.0	[64]
AChE-MWCNTs/GONRs/GCE	0.0017	0.005–5.0	[65]
AChE/PDDA-MWCNTs-GR/GCE	0.001	0.255–14.9	[66]
MWCNT/PANI/AChE	1.4	9.9–49.6	[67]
GO-IL/GCE	0.02	0.1–12.0	[68]
ZXCPE	0.3	1–100	[69]
CB-NP electrode	12	25–125	[70]
IL/CC	1.4	10–75	[71]
AChE/COF _{Thi-TFPB} /GCE	0.22	2.2–60	This work

3.5. Detection of Carbaryl in Vegetable Samples

In addition, the AChE/COF_{Thi-TFPB}/GCE sensor and high-performance liquid chromatography (HPLC) were used to detect carbaryl in real samples to demonstrate the practical application capability of the sensor. Firstly, a 100 g lettuce sample was chopped and put into a juicer containing 100 mL of 0.1 M PBS (pH = 7.0). Then, the obtained mixture was filtered, and the filtrate was used as the actual sample. Next, different concentrations of carbaryl were added to the actual sample, and the carbaryls in the actual samples were determined by the AChE/COF_{Thi-TFPB}/GCE sensor and HPLC. The obtained results are shown in Table 2. It could be seen that the carbaryl content in the actual samples obtained by the AChE/COF_{Thi-TFPB}/GCE sensor was close to the results of the HPLC test, which proved that the AChE/COF_{Thi-TFPB}/GCE sensor has the potential to detect carbaryl in real examples.

Table 2. The detection of carbaryl in lettuce juice by AChE/COF_{Thi-TFPB}/GCE and HPLC.

Sample	Added (μM)	Found (μM)	Average Value (μM)	Recovery (%)	RSD (% , $n = 3$)	HPLC (μM)	RSD (% , $n = 3$)
1	0	-	-	-	-	-	-
2	5	4.85, 5.03, 4.96	4.95	99	1.8	4.98	1.8
3	10	10.2, 10.8, 9.8	10.27	102.7	4.9	10.33	4.9
4	20	20.7, 20.1, 20.5	20.4	102	1.5	20.45	1.5

4. Conclusions

The development of efficient, good, stable and reproducible AChE inhibition-based electrochemical biosensors might rely on the immobilization of the enzyme on suitable support materials and the introduction of internal reference signals to eliminate irrelevant effects in detection. In this work, a ratiometric electrochemical sensor was constructed by using the positively charged COF_{Thi-TFPB} with an inert redox peak as the support material to load the AChE enzyme. The COF_{Thi-TFPB} could immobilize the AChE enzyme and maintain its activity. On the other hand, its inherent redox peak at 0/−0.22 V was inert to the detection of carbaryl, which could be used as a reference signal to further improve the sensitivity and accuracy of the detection. The linear range of this sensor was 2.2–60 μM , the detection limit was 0.22 μM , and it had good selectivity, reproducibility and stability. This suggests that this material has the potential to be applied to detect low-level pesticide residues.

Author Contributions: Y.L. and G.M. conceived and planned the study. Y.L., N.W. and L.W. carried out the experiments. Y.L., Y.S. and Y.D. writing—review and editing the manuscript. G.M. was responsible for supervision, project administration and funding acquisition. All authors provided critical feedback and helped shape the research, analysis. All authors have read and agreed to the published version of the manuscript.

Funding: This work was financially supported by the National Natural Science Foundation of China (21964010).

Institutional Review Board Statement: Not applicable.

Informed Consent Statement: Not applicable.

Data Availability Statement: The data is available under the request to the correspondence.

Conflicts of Interest: The authors declare no conflict of interest.

References

1. Nunes, E.; Silva, M.; Rascon, J.; Leiva-Tafur, D.; Lapa, R.; Cesarino, I. Acetylcholinesterase biosensor based on functionalized renewable carbon platform for detection of carbaryl in food. *Biosensors* **2022**, *12*, 486. [[CrossRef](#)] [[PubMed](#)]
2. Raymundo-Pereira, P.A.; Gomes, N.O.; Shimizu, F.M.; Machado, A.S.; Oliveira, O.N., Jr. Selective and sensitive multiplexed detection of pesticides in food samples using wearable, flexible glove-embedded non-Enzymatic Sensors. *Chem. Eng. J.* **2021**, *408*, 127279. [[CrossRef](#)]
3. Paschoalin, R.T.; Gomes, N.O.; Almeida, G.F.; Bilatto, S.; Farinas, C.S.; Machado, S.A.S.; Mattoso, L.H.C.; Oliveira, O.N., Jr.; Raymundo-Pereira, P.A. Wearable sensors made with solution-blow spinning poly (lactic acid) for non-enzymatic pesticide detection in agriculture and food safety. *Biosens. Bioelectron.* **2022**, *199*, 11385. [[CrossRef](#)] [[PubMed](#)]
4. Umaphathi, R.; Sonwal, S.; Lee, M.; Rani, G.; Lee, E.; Jeon, T.; Kang, S.; Oh, M.; Huh, Y. Colorimetric based on-site sensing strategies for the rapid detection of pesticides in agricultural foods: New horizons, perspectives, and challenges. *Coord. Chem. Rev.* **2021**, *446*, 214061. [[CrossRef](#)]
5. Jiang, W.; Liu, Y.; Ke, Z.; Zhang, L.; Zhang, M.; Zhou, Y.; Wang, H.; Wu, C.; Qiu, J.; Hong, Q. Substrate preference of carbamate hydrolase CehA reveals its environmental behavior. *J. Hazard. Mater.* **2021**, *403*, 123677. [[CrossRef](#)]
6. Su, D.; Zhao, X.; Yan, X.; Han, X.; Zhu, Z.; Wang, C.; Jia, X.; Liu, F.; Sun, P.; Liu, X.; et al. Background-free sensing platform for on-site detection of carbamate pesticide through upconversion nanoparticles-based hydrogel suit. *Biosens. Bioelectron.* **2021**, *194*, 113598. [[CrossRef](#)]
7. Madrigal, J.; Jones, R.; Gunier, R.; Whitehead, T.; Reynolds, P.; Metayer, C.; Ward, M. Residential exposure to carbamate, organophosphate, and pyrethroid insecticides in house dust and risk of childhood acute lymphoblastic leukemia. *Environ. Res.* **2021**, *201*, 111501. [[CrossRef](#)]
8. Chen, Z.; Wu, H.; Xiao, Z.; Fu, H.; Shen, Y.; Luo, L.; Wang, H.; Lei, H.; Hongsibsong, S.; Xu, Z. Rational hapten design to produce high-quality antibodies against carbamate pesticides and development of immunochromatographic assays for simultaneous pesticide screening. *J. Hazard. Mater.* **2021**, *412*, 125241. [[CrossRef](#)]
9. Wang, S.; Shi, X.; Liu, F.; Laborda, P. Chromatographic methods for detection and quantification of carbendazim in food. *J. Agric. Food Chem.* **2020**, *68*, 11880–11894. [[CrossRef](#)]
10. Ruengprapavut, S.; Sophonnithiprasert, T.; Pongpoungphet, N. The effectiveness of chemical solutions on the removal of carbaryl residues from cucumber and chili presoaked in carbaryl using the HPLC technique. *Food Chem.* **2020**, *309*, 125659. [[CrossRef](#)]
11. Chullasat, K.; Huang, Z.; Bunkoed, O.; Kanatharana, P.; Lee, H. Bubble-in-drop microextraction of carbamate pesticides followed by gas chromatography-mass spectrometric analysis. *Microchem. J.* **2020**, *155*, 104666. [[CrossRef](#)]
12. Mao, X.; Xiao, W.; Wan, Y.; Li, Z.; Luo, D.; Yang, H. Dispersive solid-phase extraction using microporous metal-organic framework UiO-66: Improving the matrix compounds removal for assaying pesticide residues in organic and conventional vegetables. *Food Chem.* **2021**, *345*, 128807. [[CrossRef](#)] [[PubMed](#)]
13. Zhang, D.; Liang, P.; Chen, W.; Tang, Z.; Li, C.; Xiao, K.; Jin, S.; Ni, D.; Yu, Z. Rapid field trace detection of pesticide residue in food based on surface-enhanced Raman spectroscopy. *Microchim. Acta* **2021**, *188*, 370. [[CrossRef](#)] [[PubMed](#)]
14. Wang, S.; Shi, X.; Zhu, G.; Zhang, Y.; Jin, D.; Zhou, Y.; Liu, F.; Laborda, P. Application of surface-enhanced Raman spectroscopy using silver and gold nanoparticles for the detection of pesticides in fruit and fruit juice. *Trends Food Sci. Technol.* **2021**, *116*, 583–602. [[CrossRef](#)]
15. Pu, H.; Huang, Z.; Xu, F.; Sun, D.-W. Two-dimensional self-assembled Au-Ag core-shell nanorods nanoarray for sensitive detection of thiram in apple using surface-enhanced Raman spectroscopy. *Food Chem.* **2020**, *343*, 128548. [[CrossRef](#)]
16. Zha, Y.; Li, Y.; Hu, P.; Lu, S.; Ren, H.; Liu, Z.; Yang, H.; Zhou, Y. Duplex-specific nuclease-triggered fluorescence immunoassay based on dual-functionalized AuNP for acetochlor, metolachlor, and propisochlor. *Anal. Chem.* **2021**, *93*, 13886–13892. [[CrossRef](#)]
17. Zhao, Y.; Ruan, X.; Song, Y.; Smith, J.; Vasylieva, N.; Hammock, B.; Lin, Y.; Du, D. Smartphone-based dual-channel immunochromatographic test strip with polymer quantum dot labels for simultaneous detection of cypermethrin and 3-phenoxybenzoic acid. *Anal. Chem.* **2021**, *93*, 13658–13666. [[CrossRef](#)]
18. Li, Z.; Zhou, J.; Dong, T.; Xu, Y.; Shang, Y. Application of electrochemical methods for the detection of abiotic stress biomarkers in plants. *Biosens. Bioelectron.* **2021**, *182*, 113105. [[CrossRef](#)]
19. Sinha, A.; Ma, K.; Zhao, H. 2D Ti₃C₂T_x flakes prepared by in-situ HF etchant for simultaneous screening of carbamate pesticides. *J. Colloid Interface Sci.* **2021**, *590*, 365–374. [[CrossRef](#)]
20. Wu, J.; Yang, Q.; Li, Q.; Li, H.; Li, F. Two-Dimensional MnO₂ nanozyme-mediated homogeneous electrochemical detection of organophosphate pesticides without the interference of H₂O₂ and color. *Anal. Chem.* **2021**, *93*, 4084–4091. [[CrossRef](#)]

21. Qi, J.; Tan, D.; Wang, X.; Ma, H.; Wan, Y.; Hu, A.; Li, L.; Xiao, B.; Lu, B. A novel acetylcholinesterase biosensor with dual-recognized strategy based on molecularly imprinted polymer. *Sens. Actuators B* **2021**, *337*, 129760. [[CrossRef](#)]
22. Fernandez-Ramos, M.; Ogunneye, A.; Babarinde, N.; Erenas, M.; Capitan-Vallvey, L. Bioactive microfluidic paper device for pesticide determination in waters. *Talanta* **2020**, *218*, 121108. [[CrossRef](#)] [[PubMed](#)]
23. Zhu, Y.; Wang, M.; Zhang, X.; Cao, J.; She, Y.; Cao, Z.; Wang, J.; Abd El-Aty, A. Acetylcholinesterase immobilized on magnetic mesoporous silica nanoparticles coupled with fluorescence analysis for rapid detection of carbamate pesticides. *ACS Appl. Nano Mater.* **2022**, *5*, 1327–1338. [[CrossRef](#)]
24. Loguercio, L.; Thesing, A.; Demingos, P.; de Albuquerque, C.; Rodrigues, R.; Brolo, A.; Santos, J. Efficient acetylcholinesterase immobilization for improved electrochemical performance in polypyrrole nanocomposite-based biosensors for carbaryl pesticide. *Sens. Actuators B* **2021**, *339*, 129875. [[CrossRef](#)]
25. Zhang, Y.; Liu, X.; Qiu, S.; Zhang, Q.; Tang, W.; Liu, H.; Guo, Y.; Ma, Y.; Guo, X.; Liu, Y. A flexible acetylcholinesterase-modified graphene for chiral pesticide sensor. *J. Am. Chem. Soc.* **2019**, *141*, 14643–14649. [[CrossRef](#)]
26. Li, X.; Gao, X.; Gai, P.; Liu, X.; Li, F. Degradable metal-organic framework/methylene blue composites-based homogeneous electrochemical strategy for pesticide assay. *Sens. Actuators B* **2020**, *323*, 128701. [[CrossRef](#)]
27. Chen, J.; Chen, X.; Wang, P.; Liu, S.; Chi, Z. Aggregation-induced emission luminogen@manganese dioxide core-shell nanomaterial-based paper analytical device for equipment-free and visual detection of organophosphorus pesticide. *J. Hazard. Mater.* **2021**, *413*, 125306. [[CrossRef](#)]
28. Montali, L.; Calabretta, M.; Lopreside, A.; D'Elia, M.; Guardigli, M.; Michelini, E. Multienzyme chemiluminescent foldable biosensor for on-site detection of acetylcholinesterase inhibitors. *Biosens. Bioelectron.* **2020**, *162*, 112232. [[CrossRef](#)]
29. Yu, L.; Chang, J.; Zhuang, X.; Li, H.; Hou, T.; Li, F. Two-dimensional cobalt-doped Ti₃C₂ MXene nanozyme-mediated homogeneous electrochemical strategy for pesticides assay based on in situ generation of electroactive substances. *Anal. Chem.* **2022**, *94*, 3669–3676. [[CrossRef](#)]
30. Zhu, H.; Liu, P.; Xu, L.; Li, X.; Hu, P.; Liu, B.; Pan, J.; Yang, F.; Niu, X. Nanozyme-participated biosensing of pesticides and cholinesterases: A critical review. *Biosensors* **2021**, *11*, 382. [[CrossRef](#)]
31. Rafat, N.; Satoh, P.; Worden, R. Electrochemical biosensor for markers of neurological esterase inhibition. *Biosensors* **2021**, *11*, 459. [[CrossRef](#)] [[PubMed](#)]
32. Pinyou, P.; Blay, V.; Muresan, L.; Noguier, T. Enzyme-modified electrodes for biosensors and biofuel cells. *Mater. Horiz.* **2019**, *6*, 1336–1358. [[CrossRef](#)]
33. He, Y.; Hu, F.; Zhao, J.; Yang, G.; Zhang, Y.; Chen, S.; Yuan, R. Bifunctional moderator-powered ratiometric electrochemiluminescence enzymatic biosensors for detecting organophosphorus pesticides based on dual-signal combined nanoprobe. *Anal. Chem.* **2021**, *93*, 8783–8790. [[CrossRef](#)] [[PubMed](#)]
34. Itsoponpan, T.; Thanachayanont, C.; Hasin, P. Sponge-like CuInS₂ microspheres on reduced graphene oxide as an electrocatalyst to construct an immobilized acetylcholinesterase electrochemical biosensor for chlorpyrifos detection in vegetables. *Sens. Actuators B* **2021**, *337*, 129775. [[CrossRef](#)]
35. Kadambar, V.; Bellare, M.; Bollella, P.; Katz, E.; Melman, A. Electrochemical control of the catalytic activity of immobilized enzymes. *Chem. Commun.* **2020**, *56*, 13800–13803. [[CrossRef](#)]
36. Welden, M.; Poghosian, A.; Vahidpour, F.; Wendlandt, T.; Keusgen, M.; Wege, C.; Schoning, M. Towards multi-analyte detection with field-effect capacitors modified with tobacco mosaic virus bioparticles as enzyme nanocarriers. *Biosensors* **2022**, *12*, 43. [[CrossRef](#)]
37. Arnold, J.; Chapman, J.; Arnold, M.; Dinu, C. Hyaluronic acid allows enzyme immobilization for applications in biomedicine. *Biosensor* **2022**, *12*, 28. [[CrossRef](#)] [[PubMed](#)]
38. Yang, S.; Liu, J.; Zheng, H.; Zhong, J.; Zhou, J. Simulated revelation of the adsorption behaviours of acetylcholinesterase on charged self-assembled monolayers. *Nanoscale* **2020**, *12*, 3701–3714. [[CrossRef](#)]
39. Zhang, C.; Liu, Z.; Zhang, L.; Zhu, A.; Liao, F.; Wan, J.; Zhou, J.; Tian, Y. A robust Au–C≡C functionalized surface: Toward real-time mapping and accurate quantification of Fe²⁺ in the brains of live AD mouse models. *Angew. Chem. Int. Ed.* **2020**, *59*, 20499–20507. [[CrossRef](#)]
40. Zhong, W.; Gao, F.; Zou, J.; Liu, S.; Li, M.; Gao, Y.; Yu, Y.; Wang, X.; Lu, L. MXene@Ag-based ratiometric electrochemical sensing strategy for effective detection of carbendazim in vegetable samples. *Food Chem.* **2021**, *360*, 130006. [[CrossRef](#)]
41. Yang, G.; He, Y.; Zhao, J.; Chen, S.; Yuan, R. Ratiometric electrochemiluminescence biosensor based on Ir nanorods and CdS quantum dots for the detection of organophosphorus pesticides. *Sens. Actuators B* **2021**, *341*, 130008. [[CrossRef](#)]
42. Zhang, K.; Lv, S.; Tang, D. Novel 3D printed device for dual-signaling ratiometric photoelectrochemical readout of biomarker using λ-exonuclease-assisted recycling amplification. *Anal. Chem.* **2019**, *91*, 10049–10055. [[CrossRef](#)] [[PubMed](#)]
43. Qiu, Z.; Shu, J.; Liu, J.; Tang, D. Dual-channel photoelectrochemical ratiometric aptasensor with up-converting nanocrystals using spatial-resolved technique on homemade 3D printed device. *Anal. Chem.* **2019**, *91*, 1260–1268. [[CrossRef](#)] [[PubMed](#)]
44. Zhu, L.; Zhang, M.; Ye, J.; Yan, M.; Zhu, Q.; Huang, J.; Yang, X. Ratiometric electrochemiluminescent/electrochemical strategy for sensitive detection of microRNA based on duplex-specific nuclease and multilayer circuit of catalytic hairpin assembly. *Anal. Chem.* **2020**, *92*, 8614–8622. [[CrossRef](#)] [[PubMed](#)]
45. Liu, Y.; Yang, H.; Wan, R.; Khan, M.; Wang, N.; Busquets, R.; Deng, R.; He, Q.; Zhao, Z. Ratiometric G-quadruplex assay for robust lead detection in food samples. *Biosensors* **2021**, *11*, 274. [[CrossRef](#)]

46. Zhang, G.; Chai, H.; Tian, M.; Zhu, S.; Qu, L.; Zhang, X. Zirconium-metalloporphyrin frameworks-luminol competitive electrochemiluminescence for ratiometric detection of polynucleotide kinase activity. *Anal. Chem.* **2020**, *92*, 7354–7362. [[CrossRef](#)]
47. Wang, L.; Xie, Y.; Yang, Y.; Liang, H.; Wang, L.; Song, Y. Electroactive covalent organic frameworks/carbon nanotubes composites for electrochemical sensing. *ACS Appl. Nano Mater.* **2020**, *3*, 1412–1419. [[CrossRef](#)]
48. Meng, Y.; Luo, Y.; Shi, J.; Ding, H.; Lang, X.; Chen, W.; Zheng, A.; Sun, J.; Wang, C. 2D and 3D porphyrinic covalent organic frameworks: The influence of dimensionality on functionality. *Angew. Chem. Int. Ed.* **2020**, *59*, 3624–3629. [[CrossRef](#)]
49. Liu, Y.; Ma, Y.; Zhao, Y.; Sun, X.; Gandara, F.; Furukawa, H.; Liu, Z.; Zhu, H.; Zhu, C.; Suenaga, K.; et al. Weaving of organic threads into a crystalline covalent organic framework. *Science* **2016**, *351*, 365–369. [[CrossRef](#)]
50. Liang, A.; Zhi, S.; Liu, Q.; Li, C.; Jiang, Z. A new covalent organic framework of dicyandiamide-benzaldehyde nanocatalytic amplification SERS/RRS aptamer assay for ultratrace oxytetracycline with the nanogold indicator reaction of polyethylene glycol 600 ACS. *Biosensor* **2021**, *11*, 458. [[CrossRef](#)]
51. Liang, H.; Wang, L.; Yang, Y.; Song, Y.; Wang, L. A novel biosensor based on multienzyme microcapsules constructed from covalent-organic framework. *Biosens. Bioelectron.* **2021**, *193*, 113553. [[CrossRef](#)] [[PubMed](#)]
52. Wu, N.; Wang, L.; Xie, Y.; Du, Y.; Song, Y.; Wang, L. Double signal ratiometric electrochemical riboflavin sensor based on macroporous carbon/electroactive thionine-contained covalent organic framework. *J. Colloid Interface Sci.* **2022**, *608*, 219–226. [[CrossRef](#)] [[PubMed](#)]
53. Dong, S.; Zhang, J.; Huang, G.; Wei, W.; Huang, T. Conducting microporous organic polymer with -OH functional groups: Special structure and multi-functional integrated property for organophosphorus biosensor. *Chem. Eng. J.* **2021**, *405*, 126682. [[CrossRef](#)]
54. Gutierrez-Sanchez, C.; Pita, M.; Vaz-Dominguez, C.; Shleev, S.; De Lacey, A. Gold nanoparticles as electronic bridges for laccase-based biocathodes. *J. Am. Chem. Soc.* **2012**, *134*, 17212–17220. [[CrossRef](#)]
55. Cai, C.X.; Ju, H.X.; Chen, H.Y. Electrocatalysis of poly-thionine modified microband gold electrode for oxidation of reduced nicotinamide adenine dinucleotide. *Chem. J. Chin. Univ.* **1995**, *16*, 368–372.
56. Liu, H.; Lu, X.; Xiao, D.; Zhou, M.; Xu, D.; Sun, L.; Song, Y. Hierarchical Cu–Co–Ni nanostructures electrodeposited on carbon nanofiber modified glassy carbon electrode: Application to glucose detection. *Anal. Methods* **2013**, *5*, 6360–6367. [[CrossRef](#)]
57. Huang, J.; Zhang, Y.; Deng, X.; Li, J.; Huang, S.; Jin, X.; Zhu, X. Self-encapsulated enzyme through in-situ growth of polypyrrole for high-performance enzymatic biofuel cell. *Chem. Eng. J.* **2022**, *429*, 132148. [[CrossRef](#)]
58. Wang, Y.; Zhang, X.; Zhan, Y.; Li, J.; Nie, H.; Yang, Z. Au@Fe₃O₄ nanocomposites as conductive bridges coupled with a bi-enzyme-aided system to mediate gap-electrical signal transduction for homogeneous aptasensor mycotoxins detection. *Sens. Actuators B* **2020**, *321*, 128553. [[CrossRef](#)]
59. Zeng, R.; Huang, Z.; Wang, Y.; Tang, D. Enzyme-encapsulated DNA hydrogel for highly efficient electrochemical sensing glucose. *ChemElectroChem* **2020**, *7*, 1537–1541. [[CrossRef](#)]
60. Luo, Z.; Zhang, L.; Zeng, R.; Su, L.; Tang, D. Near-infrared light-excited core–core–shell UCNP@Au@CdS upconversion nanospheres for ultrasensitive photoelectrochemical enzyme immunoassay. *Anal. Chem.* **2018**, *90*, 9568–9575. [[CrossRef](#)]
61. Wang, X.; Yang, S.; Shan, J.; Bai, X. Novel electrochemical acetylcholinesterase biosensor based on core-shell covalent organic framework@multi-walled carbon nanotubes (COF@MWCNTs) composite for detection of malathion. *Int. J. Electrochem. Sci.* **2022**, *17*, 220543. [[CrossRef](#)]
62. Da Silva, M.; Vanzela, H.; Defavari, L.; Cesarino, I. Determination of carbamate pesticide in food using a biosensor based on reduced graphene oxide and acetylcholinesterase enzyme. *Sens. Actuators B* **2018**, *277*, 555–561. [[CrossRef](#)]
63. Santos, C.S.; Mossanha, R.; Pessoa, C.A. Biosensor for carbaryl based on gold modified with PAMAM-G₄ dendrimer. *J. Appl. Electrochem.* **2015**, *45*, 325–334. [[CrossRef](#)]
64. Gong, Z.; Guo, Y.; Sun, X.; Cao, Y.; Wang, X. Acetylcholinesterase biosensor for carbaryl detection based on interdigitated array microelectrodes. *Bioprocess Biosyst. Eng.* **2014**, *37*, 1929–1934. [[CrossRef](#)] [[PubMed](#)]
65. Liu, Q.; Fei, A.; Huan, J.; Mao, H.; Wang, K. Effective amperometric biosensor for carbaryl detection based on covalent immobilization acetylcholinesterase on multiwall carbon nanotubes/graphene oxide nanoribbons nanostructure. *J. Electroanal. Chem.* **2015**, *740*, 8–13. [[CrossRef](#)]
66. Sun, X.; Gong, Z.; Cao, Y.; Wang, X. Acetylcholinesterase biosensor based on poly (diallyldimethylammonium chloride)-multi-walled carbon nanotubes-graphene hybrid film. *Nano-Micro Lett.* **2013**, *5*, 47–56. [[CrossRef](#)]
67. Cesarino, I.; Moraes, F.; Lanza, M.; Machado, S. Electrochemical detection of carbamate pesticides in fruit and vegetables with a biosensor based on acetylcholinesterase immobilised on a composite of polyaniline–carbon nanotubes. *Food Chem.* **2012**, *135*, 873–879. [[CrossRef](#)]
68. Liu, B.; Xiao, B.; Cui, L. Electrochemical analysis of carbaryl in fruit samples on graphene oxide-ionic liquid composite modified electrode. *J. Food Compos. Anal.* **2015**, *40*, 14–18. [[CrossRef](#)]
69. Salih, F.; Achiou, B.; Ouammou, M.; Bennazha, J.; Ouarzane, A.; Alami Younssi, S.; Rhazi, M.E. Electrochemical sensor based on low silica X zeolite modified carbon paste for carbaryl determination. *J. Adv. Res.* **2017**, *8*, 669–676. [[CrossRef](#)]
70. Flavio, D.; Michele, D.; Manuel, S.; Dario, C.; Alberto, E. Press-transferred carbon black nanoparticles on board of microfluidic chips for rapid and sensitive amperometric determination of phenyl carbamate pesticides in environmental samples. *Microchim. Acta* **2016**, *183*, 3143–3149.
71. Zhang, M.; Zhang, Z.; Yang, Y.; Zhang, Y.; Wang, Y.; Chen, X. Ratiometric strategy for electrochemical sensing of carbaryl residue in water and vegetable samples. *Sensors* **2020**, *20*, 1524. [[CrossRef](#)] [[PubMed](#)]